Nano Energy 125 (2024) 109604

Contents lists available at ScienceDirect

Nano Energy

journal homepage: www.elsevier.com/locate/nanoen

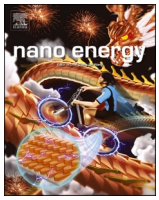

2,5-dichloro-3,4-diiodothiophene as a versatile solid additive for high-performance organic solar cells

Tianqi Chen [a], Yuyang Bai [a], Xinyi Ji [a,*], Wanying Feng [b], Tainan Duan [c,*], Xue Jiang [c], Yuan-qiu-qiang Yi [d], Jifa Yu [e], Guanghao Lu [e], Xiangjian Wan [b], Bin Kan [a,*], Yongsheng Chen [b]

[a] School of Materials Science and Engineering, National Institute for Advanced Materials, Nankai University, Tianjin 300350, China
[b] State Key Laboratory and Institute of Elemento-Organic Chemistry, Frontiers Science Center for New Organic Matter, The Centre of Nanoscale Science and Technology and Key Laboratory of Functional Polymer Materials, Renewable Energy Conversion and Storage Center (RECAST), College of Chemistry, Nankai University, Tianjin 300071, China
[c] Chongqing Institute of Green and Intelligent Technology, Chongqing School, University of Chinese Academy of Sciences (UCAS Chongqing), Chinese Academy of Sciences, Chongqing 400714, China
[d] Printable Electronics Research Center, Nano Devices and Materials Division, Suzhou Institute of Nano-Tech and Nano-Bionics, Chinese Academy of Sciences, Suzhou, Jiangsu 215123, China
[e] Institute of Science and Technology, Xi'an Jiaotong University, Xi'an 710054, China

ARTICLE INFO

Keywords:
Thiophene
Solid additives
Solar cells
High-efficiency
Morphology

ABSTRACT

Volatile solid additive (SA) with diverse chemical structures has been proved to be an alternative to prepare high-efficient organic solar cells (OSCs). While, various organic photovoltaic materials raise challenges in selecting suitable SAs during the device optimization. Herein, based on the simple and commonly used thiophene unit, we proposed a perhalogenated 2,5-dichloro-3,4-diiodothiophene (SA-T5) as the SA for the device optimizations. As results, the capacity of SA-T5 in optimizing molecular packings of small-molecular acceptor L8-BO, dimeric acceptor DL8, and polymeric acceptor PY-DT based blend films has been demonstated. Their optimized morphologies assisted by SA-T5 contribute to the suppressed charge recombination and enhanced charge transportation, resulting in their improved short-circuit current density and fill factor, simultaneously. In comparsion with as-cast devices, SA-T5-treated devices showed significantly improved power conversion efficiencies (PCEs) of 18.8 % for PM6:L8-BO, 17.8 % for PM6:DL8, and 17.6 % for PM6:PY-DT, respectively. Furthermore, the potential of SA-T5 in obtaining high-performance ternary OSCs was also confirmed, for example, a 18.1 % efficiency was realized in PM6:DL8:L8-BO based device. To our knowledge, the performance of these SA-T5-treated devices reaches the best results of different acceptor-based OSCs. Importantly, this work provides a rare and successful case to develop versatile SAs for high-performance OSCs.

1. Introduction

Organic solar cells (OSCs) have attracted considerable attention because of their flexible, lightweight nature, and promising potential applications [1–6]. The rapid and ongoing advancement of diverse photoactive materials has propelled the power conversion efficiency (PCE) of single-junction OSCs close to 20 % to date [7–9]. This progress shows a promising future for OSCs in practical applications. To prepare high-performance OSCs, it is essential to develop photoactive materials and precisely regulate the morphology of donor:acceptor (D:A) blend films [10,11]. Fine-tuning the microstructure morphology of bulk heterojunction (BHJ) by introducing a third component along with various post-treatments, such as additives, thermal annealing [12], and solvent vapor annealing [13], is crucial for achieving efficient photoelectric conversion processes and high-performance OSCs [14]. The additive strategy is currently one of the simplest yet most vital approaches to optimize the active layer morphology and achieve favorable phase separation [15].

Solvent additives such as 1,8-diiodooctane (DIO) and 1-chloronaphthalene (1-CN) with high boiling point, are commonly used to enhance the performance of OSCs by influencing the film formation process [16]. However, the completely removing these additives presents a significant challenge, requiring a time-consuming process to avoid potential damage to the morphology of BHJ blends. This challenge also raises concerns

* Corresponding authors.
E-mail addresses: xyji06@nankai.edu.cn (X. Ji), tnduan@cigit.ac.cn (T. Duan), kanbin04@nankai.edu.cn (B. Kan).

https://doi.org/10.1016/j.nanoen.2024.109604
Received 14 March 2024; Received in revised form 6 April 2024; Accepted 9 April 2024
Available online 10 April 2024

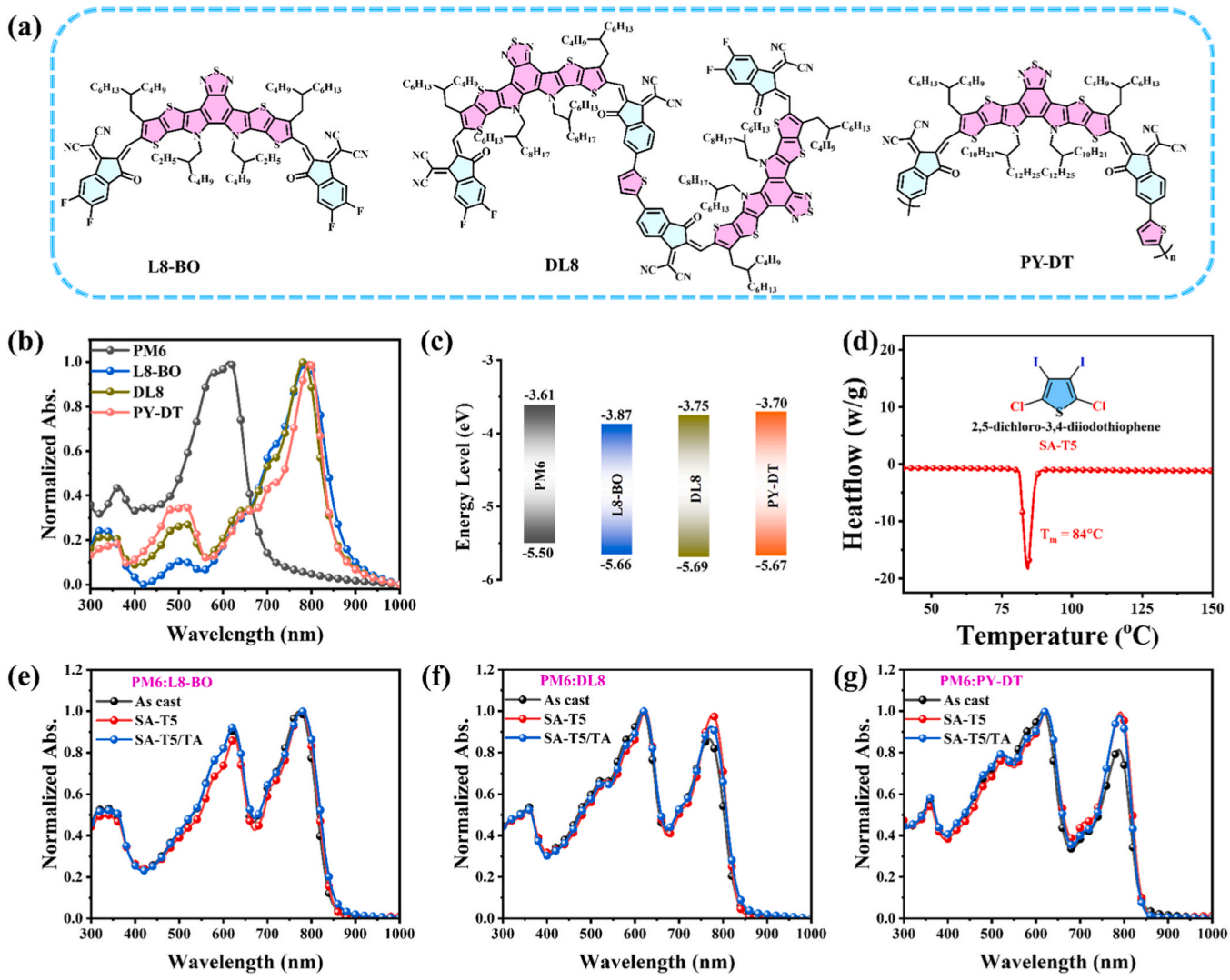

Fig. 1. a) Chemical structures of L8-BO, DL8, and PY-DT, respectively. b) Normalized absorption spectra of PM6, L8-BO, DL8, and PY-DT in their neat films. c) Energy levels of used electron donor and acceptor materials. d) DSC plot of SA-T5 and chemical structure of SA-T5. Normalized absorption spectra of e) PM6:L8-BO, f) PM6:DL8, and g) PM6:PY-DT blend films under different treatment, respectively.

about the long-term stability and reproducibility of device fabrication, which can be compromised by even trace amounts of residual additives [17]. As an alternative, the strategy of using volatile solid additive (SA) has been introduced to guarantee complete removal of additives from the active layers through the post-thermal-annealing (TA) process [18]. Several SAs with distinct chemical structures have been designed and employed to control the molecular packing and crystallinity of polymer donors and small-molecular acceptors (SMA), thereby enhancing the performance of organic solar cells [19]. For instance, Hou et al. developed a series of volatile small molecules as SAs to enhance the intermolecular π–π stacking between the polymer donor and the SMA [20]. This improvement in charge transport within the blend film led to a notable increase in PCE. The incorporation of the solid additive 1, 3-dibromo-5-chlorobenzene (DCBB) substantially enhanced the performance of PBQx-TF:eC9–2Cl-based binary device, achieving a high PCE of 19.2 % [15]. Additionally, Sun et al. introduced the solid additive 2-methoxynaphthalene (2-MN), which effectively controlled the aggregation of PM6 and polymerized small-molecular acceptor (PSMA) PY-DT. This strategic manipulation resulted in a high efficiency of 17.32 % for PM6:PY-DT-based all-polymer solar cells [21]. Recently, polymer donor:oligomer acceptor-based devices have advanced rapidly, achieving PCEs over 18 % [22–25]. Generally, the selection of additives for these blends draws from previously–used common additives, including 1-CN and 1,4-diiodobenzene.

During device fabrication, the complexity of selecting an effective SA across different systems is often due to the diversity of donor/acceptor molecular structures. Developing universal SAs that can optimize various acceptor-based blends is a challenge. Besides, such universal SAs would streamline and accelerate the morphological optimizations for high-performance OSCs [26]. Fortunately, all high-performance organic photovoltaic materials share a common and simple structural unit, namely, thiophene [27]. Compared to the benzene ring, the thiophene unit not only exhibits enhanced reactivity, enabling diverse structural modifications to suit various photovoltaic systems, but it also readily participates in favorable π–π interactions with high-performance photovoltaic molecules (PM6, Y6, etc.) [28]. These interactions may lead to more ordered molecular packing, thereby potentially enhancing PCE [29]. Most recently, we have developed a series of perhalogenated thiophenes, incorporating Br and I atoms, to regulate the morphologies of a PM6:PY-IT-based all-polymer blend [30]. While these devices have achieved PCEs over 18 %, the high thermal-annealing temperatures required (over 130℃) inevitably lead to energy waste and restrict their application in SMA-based blends.

Based on the aforementioned considerations, we have designed and

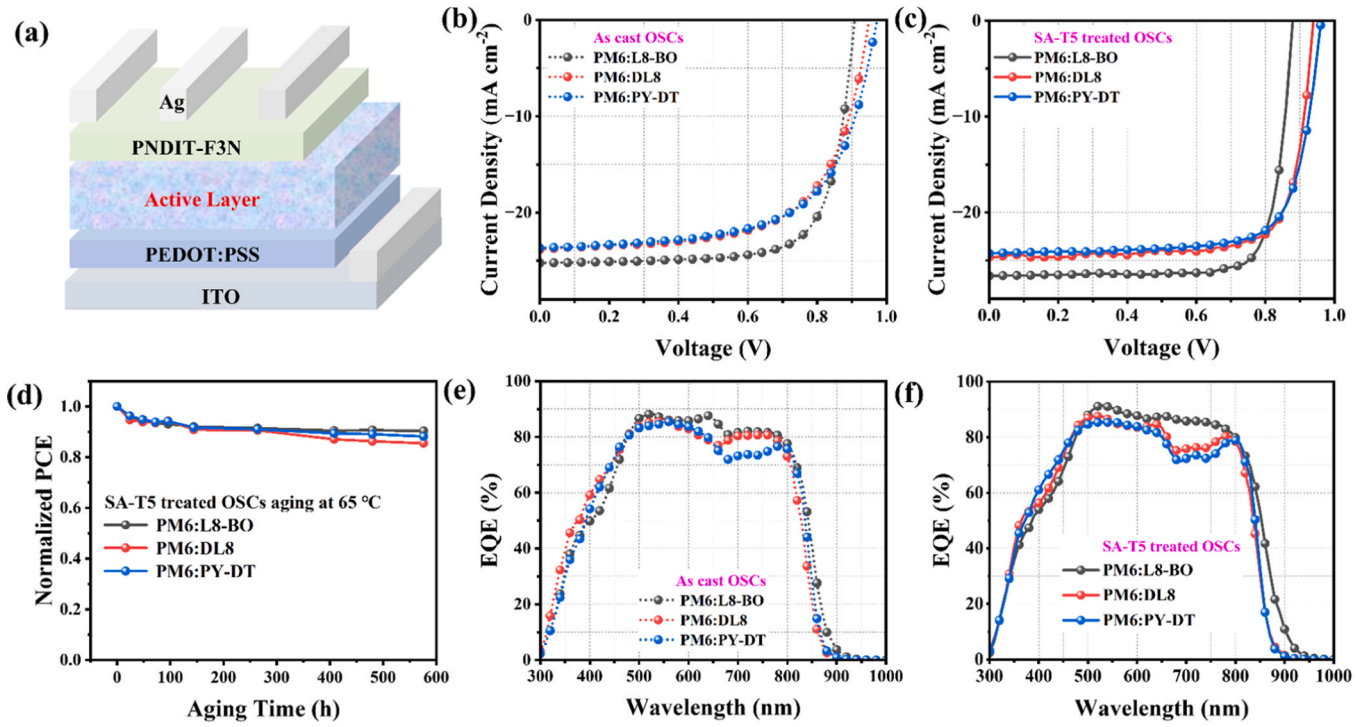

Fig. 2. a) Illustration of the adopted conventional device structure. b) *J*-V curves of as-cast OSCs. c) *J*-V curves of SA-T5 treated OSCs. d) Thermal stability of SA-T5 treated OSCs. e) EQE curves of as-cast OSCs. f) EQE curves of SA-T5 treated OSCs.

reported 2,5-dichloro-3,4-diiodothiophene (SA-T5) as a versatile solid additive for SMA, dimeric acceptor (DMA), and PSMA-based OSCs. SA-T5 presents a low melting point of 84℃, allowing for its easy and complete removal under a low thermal annealing temperature of 90℃. In this study, we selected three typical blends, PM6:L8-BO, PM6:DL8, and PM6:PY-DT, to demonstrate the universality of our newly developed SA-T5. Through systematic characterization, we found that SA-T5 effectively optimizes the active layer morphology across different acceptor types. Compared to the as-cast devices, SA-T5-treated devices showed remarkable PCEs of 18.8 %, 17.8 %, and 17.6 % for PM6:L8-BO, PM6:DL8, and PM6:PY-DT blends, respectively, highlighting the effectiveness of SA-T5 in enhancing device performance. Moreover, a remarkable PCE of over 18 % was achieved for PM6:DL8:L8-BO-based ternary OSC. To the best of our knowledge, these achieved PCEs are among the highest reported for SMA, DMA, and PSMA-based binary or ternary devices [31–33]. The broad application of SA-T5 underscores the significant potential of thiophen-based simple SAs additives in advancing the development of high-performance OSCs.

2. Results and discussion

Fig. 1a presents a series of nonfullerene acceptors, which are small-molecular acceptor L8-BO [34], dimeric acceptor DL8 [35], and polymeric acceptor PY-DT [36]. When paired with the wide bandgap polymer donor PM6, these acceptors offer complementary absorption characteristics spanning from 300–900 nm (Fig. 1b). Their energy levels in the thin-film state are estimated by the cyclic voltammetry method, and the resultant curves are plotted in Figure S1. As shown in Fig. 1c, the appropriate HOMO/LUMO energy offsets between PM6 and these acceptors provide sufficient driving forces for exciton dissociations, which is a prerequisite for realizing efficient OSCs. Additionally, the LUMO energy levels of L8-BO, DL8, and PY-DT are −3.87, −3.75 and −3.70 eV, respectively, which is progressively elevated. This gradation influences the open circuit voltages (V_{OC}) of the corresponding devices. Generally, the morphology of PM6:L8-BO, PM6:DL8, and PM6:PY-DT blend films strongly influenced by the chemical structures of the respective acceptors. In pursuit of a versatile solid additive, SA-T5 was synthesized from commercially available materials in a single step on a large scale (Scheme S1). Differential scanning calorimetry (DSC) measurements indicate that the melting point of SA-T5 is 84℃ (Fig. 1d), which facilitates its easy removal through thermal annealing.

Figure S2 displays the Fourier transform infrared (FTIR) spectra of SA-T5, which exhibits a characteristic peak at 1028 cm^{-1}. Note that blends of PM6:L8-BO, PM6:DL8, and PM6:PY-DT with SA-T5 all exhibit peaks corresponding to SA-T5 and show varying degrees of peak displacement (from 1038–1036 cm^{-1}) validating the interactions between interactions the blends and the solid additive [37]. As expected, the peak disappeared after thermal annealing, indicating that SA-T5 was

Table 1
Photovoltaic parameters of PM6:L8-BO, PM6:DL8, and PM6:PY-DT based as-cast and SA-T5 treated devices, respectively. The average values are obtained from 10 individual devices.

BHJ	Tteatment	V_{oc} (V)	J_{sc} (mA cm^{-2})	J_{sc}^{cal} (mA cm^{-2})	FF%	PCE %
PM6:L8-BO	As cast	0.908 (0.904 ±0.007)	25.22 (25.11 ±0.15)	24.22	73.9 (73.7 ±0.2)	16.9 (16.7 ±0.2)
	SA-T5	0.879 (0.874 ±0.008)	26.65 (26.49 ±0.22)	25.51	80.3 (79.6 ±0.9)	18.8 (18.6 ±0.2)
PM6:DL8	As cast	0.949 (0.950 ±0.003)	23.83 (23.57 ±0.32)	23.11	63.7 (63.1 ±1.0)	14.4 (14.2 ±0.2)
	SA-T5	0.939 (0.933 ±0.008)	24.67 (24.46 ±0.25)	23.63	76.9 (76.0 ±1.0)	17.8 (17.5 ±0.3)
PM6:PY-DT	As cast	0.973 (0.962 ±0.012)	23.69 (23.45 ±0.27)	22.81	62.9 (62.3 ±0.7)	14.5 (14.3 ±0.3)
	SA-T5	0.957 (0.955 ±0.007)	24.24 (24.25 ±0.10)	23.45	75.8 (75.0 ±1.0)	17.6 (17.5 ±0.1)

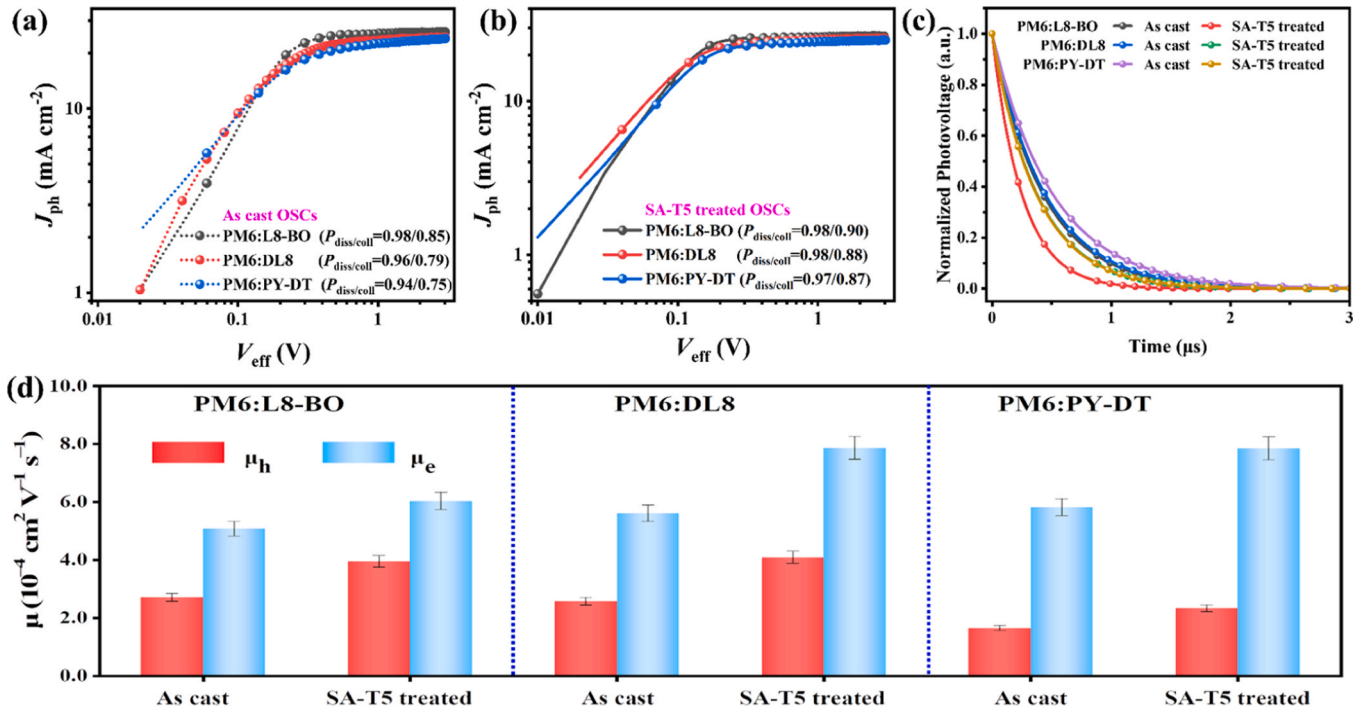

Fig. 3. J_{ph} - V_{eff} curves of a) as-cast and b) SA-T5 treated OSCs, respectively. c) TPC curves, and d) hole and electron mobility of PM6:L8-BO, PM6:DL8, and PM6:PY-DT based as-cast and SA-T5 treated devices, respectively.

completely removed following a brief thermal annealing at 90℃. The interactions between the blends and SA-T5 are further confirmed by analyzing the peaks in the ultraviolet–visible (UV–vis) absorption spectra of treatment-free, SA-T5-processed, and SA-T5-processed/TA films. A slight red shift is observed after incorporating SA-T5 into the blends, as demonstrated in Fig. 1e–g. The inclusion of the solid additive SA-T5 likely facilitates molecular stacking, which in turn improves light utilization and enhances the photocurrent density of OSCs.

To evaluate the effect of the solid additive on photovoltaic performance, OSCs were fabricated using a conventional device architecture comprising ITO/PEDOT:PSS/active layer/PNDIT-F3N/Ag (Fig. 2a). The fabrication details are provided in the Supporting Information, and the corresponding device parameters are listed in Table S1. The current density−voltage ($J-V$) characteristics of the as-cast devices for PM8:L8-BO, PM6:DL8, and PM6:PY-DT as well as the SA-T5-treated optimal devices are plotted in Figs. 2b and 2c, respectively. The optimal photovoltaic parameters summarized in Table 1 show that the PM6:L8-BO as-cast device achieved a PCE of 16.9 %, aligning with previously reported results [38]. Following SA-T5 treatment, the device exhibited a significant increase in short-circuit current (J_{SC}) from 25.22 to 26.65 mA cm^{-2} and fill factor (*FF*) from 73.9 % to 80.3 % leading to a high PCE of 18.8% for L8-BO-based devices. This performance is comparable to or even better than that of most reported PM6:L8-BO-based binary devices [39]. Additionally, the SA-T5 treatment enhanced the PCEs of the PM6:DL8 and PM6:PY-DT devices attributed to the substantial increases in their J_{SC} and *FF*. Specifically, devices based on the dimeric acceptor DL8 and polymeric acceptor PY-DT achieved satisfactory PCEs of 17.8 % and 17.6 %, respectively, which are notably higher than ~14 % of their as-cast devices. It is noteworthy that 1-CN was used to optimize the PM6:L8-BO, PM6:DL8, and PM6:PY-DT based devices, which yielded a PCE of 17.8 %, 17.5 %, and 16.5 % (Figure S3 and Table S2), respectively. Besides, similar trends were demonstrated for three devices when adopting perchlorothiophene as the additive. It is clearly that these results are obviously lower than those of SA-T5-treated devices, highlighting the superiority of our developed SA-T5. Lastly, the PM6:DL8:L8-BO ternary device, treated with SA-T5, attained a PCE of 18.1 %, representing the highest performance among dimeric acceptor-based devices with PCEs >18 % [40–42]. Based on these results, our developed SA-T5 remarkably enhances the photovoltaic properties of devices based on small-molecular, dimeric and polymeric acceptors. This implies that SA-T5 has the potential to be broadly applied in tuning the properties of various organic photovoltaic materials. In addition to PCEs, thermal stability is imperative for future applications. As shown in Fig. 2d, all optimal binary devices maintained >85 % of their original PCEs after thermal aging for over 550 h under consecutive heating at 65℃ in a nitrogen-filled glovebox, indicating the decent thermal stability of SA-T5-treated devices.

One factor contributing to the improved PCEs of SA-T5-treated devices is the enhancement of their J_{SC} values. To further confirm these findings, external quantum efficiency (EQE) measurements were performed for all devices. The corresponding EQE curves for the as-cast and SA-treated devices are presented in Figs. 2e and 2f, respectively. The integrated J_{SC} values of the PM6:L8-BO, PM6:DL8, and PM6:PY-DT as-cast devices are 24.22, 23.11, and 22.81 mA cm^{-2}, respectively. After SA-T5 treatment, the photoelectron response of the three devices exhibited a similar trend, with each showing stronger EQE response compared to their as-cast devices. This resulted in increases of 1.29, 0.52, and 0.64 mA cm^{-2} in the integrated J_{SC} values of the PM6:L8-BO, PM6:DL8, and PM6:PY-DT devices, respectively. These results indicate a more efficient photoelectric conversion process in the SA-T5-treated devices, leading to higher J_{SC} values. Additionally, the integrated J_{SC} values are within 5 % mismatch with their J_{SC} values form $J-V$ curves, confirming the enhancement of J_{SC} values for all SA-T5-treated devices. Moreover, SA-T5 treatment has a negligible impact on the value of V_{oc}. According to the Shockley–Queisser (SQ) limit theory [43], the energy losses (E_{loss}) of all devices were calculated (Figure S4 and S5) and analyzed, and the detailed results are summarized in Table S3. Compared to the as-cast devices, the SA-T5-treated devices exhibited almost identical E_{loss}, including radiative recombination loss (ΔE_2) and non-radiative recombination loss (ΔE_3). The negligible impact of SA-T5 on the E_{loss} of the corresponding devices helps to maintain their considerably high V_{oc} values, which is one of the most important preconditions for exceptional PCEs.

Subsequently, to elucidate the intrinsic mechanism of SA-T5 in

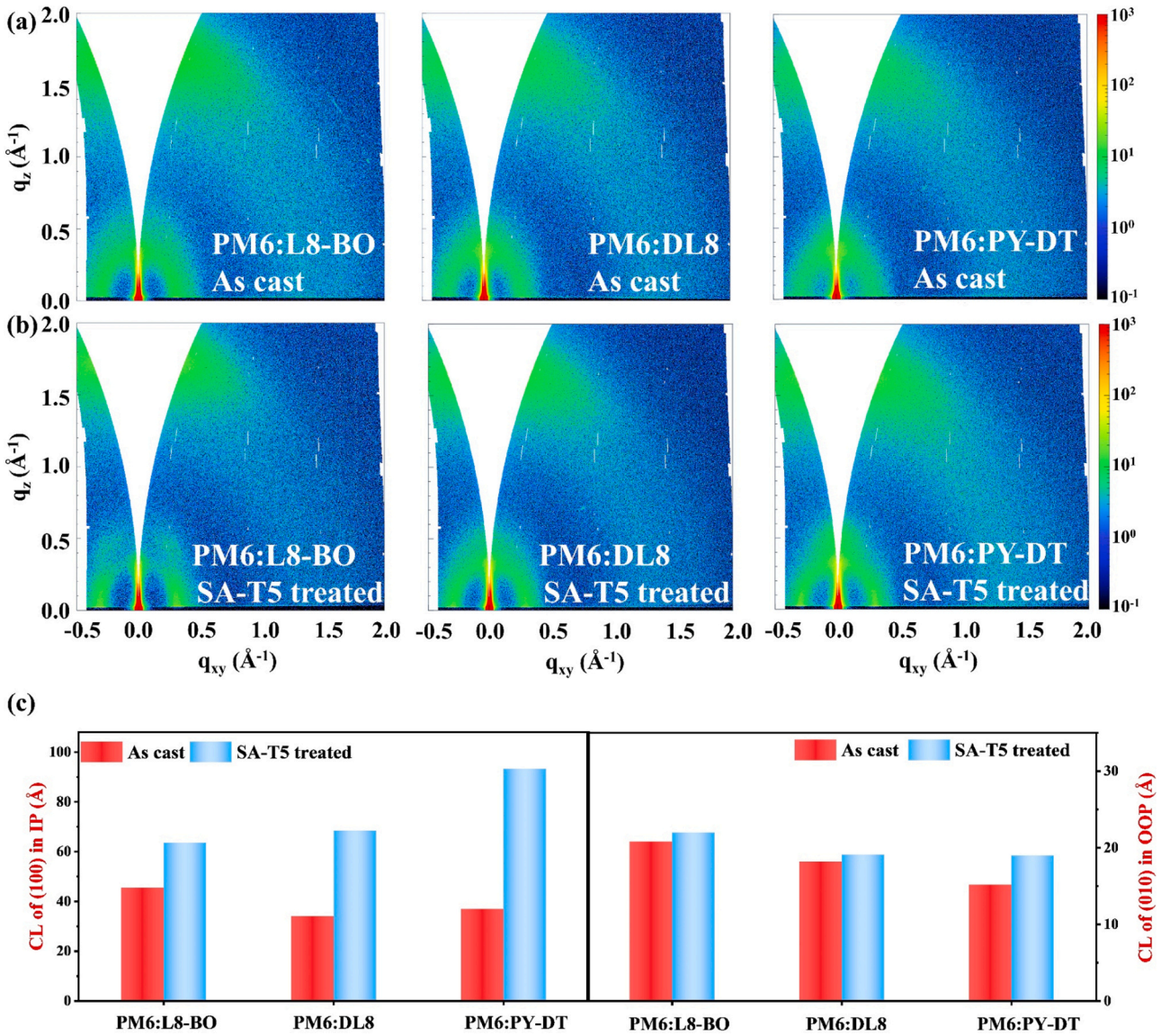

Fig. 4. a) GIWAXS images of as cast blend films. b) GIWAXS images of SA-T5 treated blend films. c) Coherence length (CLs) of (100) and (010) for three blend films under as-cast and SA-T5 treatment.

tuning the performance of these OSCs, we investigated their charge recombination dynamics and charge carrier transport properties. Fig. 3a and b show the relationship between photocurrent density (J_{ph}) and effective voltage (V_{eff}), as determined by following the reported methods [44]. Generally, compared to the as-cast devices of L8-BO, DL8, and PY-DT, all the SA-T5-processed devices demonstrated slightly higher exciton dissociation probabilities (P_{diss}), which are 0.98, 0.98 and 0.97, respectively. Furthermore, the exciton collection probabilities (P_{coll}) for PM6:L8-BO, PM6:DL8, and PM6:PY-DT SA-T5-treated devices, calculated as the ratio of J_{ph} under the maximum power output condition to the saturation current density (J_{sat}), are 0.90, 0.88, and 0.87, respectively. These values are higher than those of the corresponding as-cast devices which are 0.85, 0.79, and 0.75, respectively. Therefore, compared to all as-cast devices, the SA-T5-treated devices exhibited more efficient charge generation and collection processes, contributing to their substantially improved J_{SC} and *FF* values.

The transient photocurrent (TPC) decay method was adopted to reveal the effect of SA-T5 on charge generation (Fig. 3c). As summarized in Table S4, the charge extraction times (τ) of the PM6:L8-BO, PM6:DL8, and PM6:PY-DT as-cast devices are 0.59, 0.66, and 0.69 μs, respectively. Following SA-T5 treatment, all optimal devices exhibited faster charge extractions, evidenced by their reduced τ of 0.41, 0.56, and 0.52 μs, respectively. Enhanced P_{coll} is usually attributed to the high and balanced charge transport properties of BHJ composites. Consequently, the space charge limited current (SCLC) method, involving the fabrication of hole-only and electron-only devices, was utilized to measure their hole (μ_h) and electron (μ_e) mobility under various treatments. The calculated μ_h and μ_e values, displayed in Fig. 3d, indicate that all SA-T5-treated devices exhibit by higher hole and electron mobility compared to their corresponding as-cast devices. Using PM6:L8-BO as an example, the as-cast device obtained μ_h of 5.08×10^{-4} cm^2 V^{-1} s^{-1} and μ_e of 2.71×10^{-4} cm^2 V^{-1} s^{-1}, respectively. The results improved to 6.03×10^{-4} and 3.95×10^{-4} cm^2 V^{-1} s^{-1} after SA-T5-based treatment. Additionally, the ratio of μ_h/μ_e was reduced from 1.87 for the as-cast device to 1.53 for the SA-T5-treated device, indicating a more balanced charge transport behavior. Similar results were observed for the other two blends, PM6:DL8 and PM6:PY-DT, which explains the increased *FF* and J_{SC} of SA-T5-treated devices. These results imply that the SA-T5-based treatment is beneficial for optimizing the charge generation and charge recombination dynamics, which are usually closely related to their morphological features, as discussed below.

Atomic force microscopy (AFM) was used to assess the impact of the

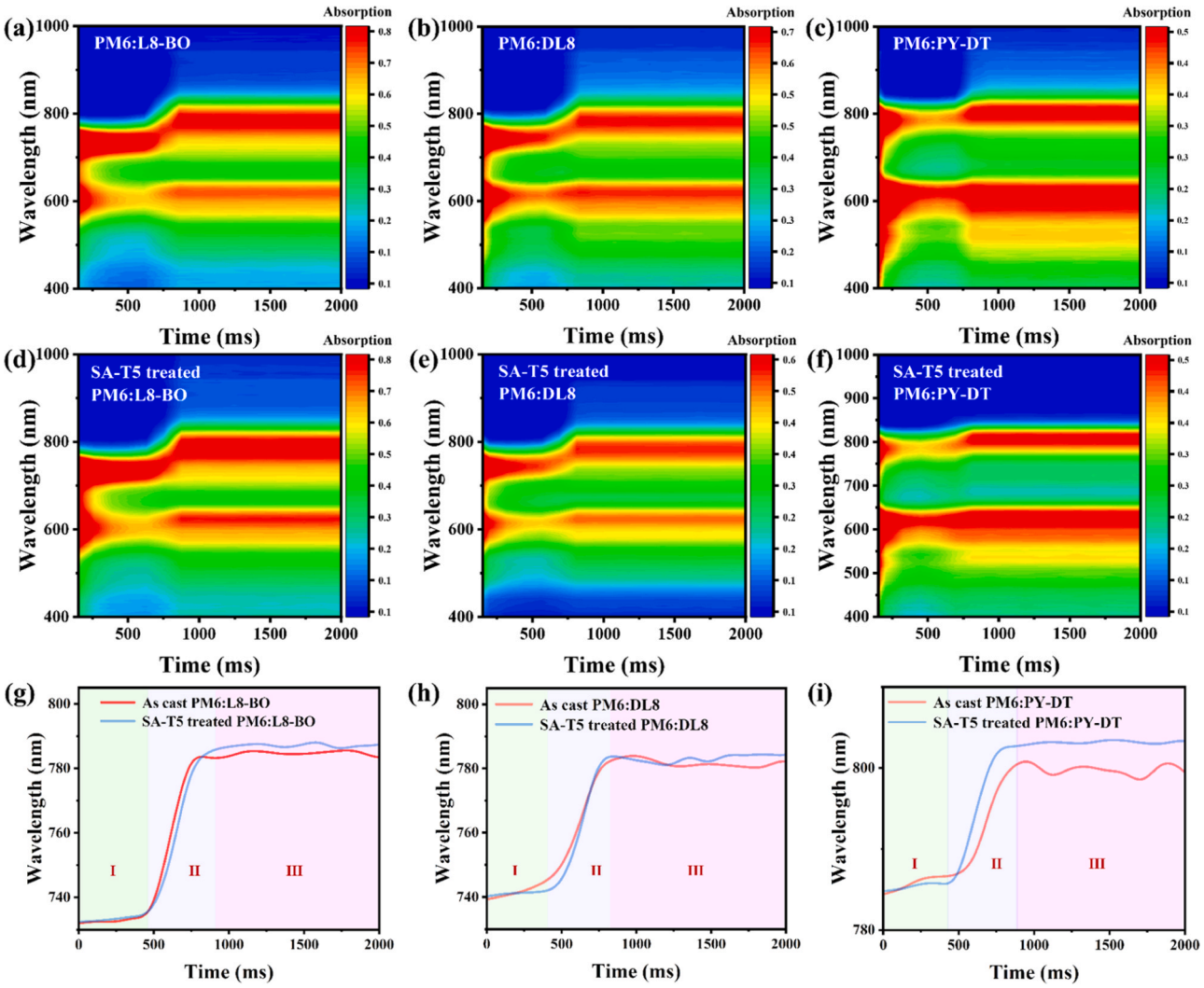

Fig. 5. (a-f) The color mapping of in situ UV–vis reflectance spectra as a function of spin-coating time, (g-i) in situ absorption location as a function of spin-coating time.

SA-T5-based treatment on the morphological features (Figures S7 and S8), which are directly linked to device performance. All blend films with and without SA-T5 treatment feature smooth surfaces with small root-mean-square roughness (R_q) below 1 nm. Compared to the as-cast films, the SA-T5-treated demonstrate more consecutive and proper D–A phase separation. The smooth surface together with distinctive fibril-like phase separations, are beneficial for establishing better contact with the electron transport layer and thereby facilitating more efficient charge transport/collection. This supports the observed increased charge mobility and *FF*.

Additionally, grazing incidence wide-angle X-ray scattering (GIWAXS) measurements were conducted to investigate the influence of SA-T5 on molecular stacking behaviors [45]. Fig. 4 illustrates the GIWAXS diffraction patterns, and Figure S9 presents the associated line-cut profiles in the in-plane (IP) and out-of-plane (OOP) directions, while Table S5 presents the corresponding parameters. All organic photovoltaic materials exhibited a preference for face-on molecular orientations within the blends, as evidenced by their sharp (100) diffraction peaks in the IP direction and (010) diffraction peaks in the OOP direction. Such molecular packing orientations are considered beneficial for charge transport in the active layers. Meanwhile, using the Scherrer equation [46], the coherence lengths (CLs) were calculated to be 20.8/22.0, 18.2/19.1, and 15.2/19.0 for as-cast/SA-T5-treated L8-BO, DL8, and PY-DT-based blend films, respectively. These results indicate that the addition of SA-T5 enhances molecular packing and improves crystallinity, which in turn facilitates charge extraction and transport, thereby contributing to the increased *FF* and J_{SC} of the devices.

In situ UV–vis absorption measurements were conducted to investigate the effect of the solid additive SA-T5 on film formation and crystallization during the spin-coating process [47,48]. Fig. 5a–f shows the color mapping of the in-situ UV–vis absorption spectra over the course of spin-coating time, and the corresponding absorption peak evolutions of representative time points for these blend films are presented in Fig. 5g–i. The film formation process can be divided into three stages. Initially, the absorption peaks of all films decreased sharply and separate into donor and acceptor parts due to a thinner liquid film. Consequently, the peak intensity and position remain stable as the solvent gradually evaporates in stage I, which represents the solution state. Second, the concentration of steadily increases to the dissolution limit as the solvent continues to evaporate. We observed that the peak intensity weakened as indicated by the contour maps and peak positions appeared to have a considerable redshift. This shift is attributed to the aggregations of donor and acceptor molecules initiating the liquid–solid transition. In Stage III, the solvent has fully evaporated to form the films, resulting in constant peak positions and intensity. Compared to the as-cast films, the peak locations of SA-T5-treated films exhibit a slight redshift, from 785 to 787 nm for L8-BO, 781 to 783 nm for DL8, and 799 to 803 nm for

PY-DT. These shifts demonstrate that the addition of a solid additive reinforces the interactions between the donor and acceptor, thereby enhancing the aggregation and crystallization. This finding is consistent with the GIWAXS results.

3. Conclusion

In this study, we have designed and synthesized a perhalogenated 2,5-dichloro-3,4-diiodothiophene (SA-T5) characterized by a low melting point and high volatility. This additive effectively manipulates the molecular packing behaviors of organic photovoltaic materials, thereby infuencing the final morphological features of active layers. The utilization of SA-T5 enables the manipulation of morphology and enhancement of molecular crystallinity across various blends, including SMA, DMA, and PSMA-based D-A blends. Consequently, in all SA-T5-treated devices exhibited improved exciton dissociation and charge transport behaviors occurred. Compared to the as-cast devices, all SA-T5-treated devices showed almost unchanged E_{loss} together along with remarkably improved J_{SC} and FF values, contributing to much higher PCEs after SA-T5 treatment, such as from 16.9 % to 18.8 % for PM6:L8-BO, from 14.4 % to 17.8 % for PM6:DL8, and from 14.5 % to 17.6 % for PM6:PY-DT. In addition, the versatility of SA-T5 in the PM6:DL8:L8-BO ternary blend was also demonstrated, achieving a satisfactory PCE over 18% for dimeric-based devices. Note that the performance of all these binary and ternary devices ranks among the best in small-molecular, dimeric, and polymeric acceptor-based OSCs, respectively. These impressive results validate the universal applicability of SA-T5 as a volatile solid additive for various high-performance OSCs. To our knowledge, solid additives that can optimize the performance across SMA to DMA to PSMA are seldom reported. Our work provides a straightforward method for selecting additives that optimize OSC morphology and has significant implications for solid additives with simple structures and broad universality.

CRediT authorship contribution statement

Yuyang Bai: Investigation, Data curation. **Yongsheng Chen:** Writing – review & editing, Supervision, Funding acquisition, Conceptualization. **Tianqi Chen:** Writing – original draft, Investigation, Formal analysis, Data curation. **Bin Kan:** Writing – review & editing, Supervision, Funding acquisition, Formal analysis, Conceptualization. **Xiangjian Wan:** Writing – review & editing, Supervision, Funding acquisition, Conceptualization. **Guanghao Lu:** Investigation, Conceptualization. **Jifa Yu:** Investigation, Data curation. **Yuan-qiu-qiang Yi:** Investigation, Data curation. **Xue Jiang:** Investigation. **Tainan Duan:** Writing – review & editing, Investigation, Conceptualization. **Wanying Feng:** Methodology, Investigation. **Xinyi Ji:** Writing – review & editing, Supervision, Conceptualization.

Declaration of Competing Interest

The authors declare that they have no known competing financial interests or personal relationships that could have appeared to influence the work reported in this paper.

Data Availability

Data will be made available on request.

Acknowledgements

The authors gratefully acknowledge the financial support from MoST of China (2022YFB4200400, 2019YFA0705900, 2023YFE0210400), NSFC (21935007, 52025033, 52303237, and 22361132530) and Natural Science Foundation of Chongqing (CSTB2023NSCQMSX0268). The authors are grateful for the technical support for Nano-X from Suzhou Institute of Nano-Tech and Nano-Bionics, Chinese Academy of Sciences (SINANO).

Appendix A. Supporting information

Supplementary data associated with this article can be found in the online version at doi:10.1016/j.nanoen.2024.109604.

References

[1] Y. Lin, H. Skaff, T. Emrick, A.D. Dinsmore, T.P. Russell, Nanoparticle assembly and transport at liquid-liquid interfaces, Science 299 (2003) 226–229, https://www.science.org/doi/abs/10.1126/science.1078616.
[2] G. Li, R. Zhu, Y. Yang, Polymer solar cells, Nat. Photonics 6 (2012) 153–161, https://doi.org/10.1038/nphoton.2012.11.
[3] J. Yuan, Y. Zhang, L. Zhou, G. Zhang, H.-L. Yip, T.-K. Lau, X. Lu, C. Zhu, H. Peng, P. A. Johnson, M. Leclerc, Y. Cao, J. Ulanski, Y. Li, Y. Zou, Single-junction organic solar cell with over 15% efficiency using fused-ring acceptor with electron-deficient core, Joule 3 (2019) 1140–1151, https://doi.org/10.1016/j.joule.2019.01.004.
[4] B.B. Fan, X.Y. Du, F. Liu, W.K. Zhong, L. Ying, R.H. Xie, X.F. Tang, K. An, J.M. Xin, N. Li, W. Ma, C.J. Brabec, F. Huang, Y. Cao, Fine-tuning of the chemical structure of photoactive materials for highly efficient organic photovoltaics, Nat. Energy 3 (2018) 1051–1058, https://doi.org/10.1038/s41560-018-0263-4.
[5] Z. Wang, Y. Bo, P. Bai, S. Zhang, G. Li, X. Wan, Y. Liu, R. Ma, Y. Chen, Self-sustaining personal all-day thermoregulatory clothing using only sunlight, Science 382 (2023) 1291–1296, https://www.science.org/doi/abs/10.1126/science.adj3654.
[6] B. Li, X. Yang, S. Li, J. Yuan, Stable block copolymer single-material organic solar cells: progress and perspective, Energy Environ. Sci. 16 (2023) 723–744, https://doi.org/10.1039/D2EE03082A.
[7] L. Wang, C. Chen, Y. Fu, C. Guo, D. Li, J. Cheng, W. Sun, Z. Gan, Y. Sun, B. Zhou, C. Liu, D. Liu, W. Li, T. Wang, Donor–acceptor mutually diluted heterojunctions for layer-by-layer fabrication of high-performance organic solar cells, Nat. Energy (2024), https://doi.org/10.1038/s41560-023-01436-z.
[8] L. Zhu, M. Zhang, J. Xu, C. Li, J. Yan, G. Zhou, W. Zhong, T. Hao, J. Song, X. Xue, Z. Zhou, R. Zeng, H. Zhu, C.-C. Chen, R.C.I. MacKenzie, Y. Zou, J. Nelson, Y. Zhang, Y. Sun, F. Liu, Single-junction organic solar cells with over 19% efficiency enabled by a refined double-fibril network morphology, Nat. Mater. 21 (2022) 656–663, https://doi.org/10.1038/s41563-022-01244-y.
[9] T. Chen, S. Li, Y. Li, Z. Chen, H. Wu, Y. Lin, Y. Gao, M. Wang, G. Ding, J. Min, Z. Ma, H. Zhu, L. Zuo, H. Chen, 19.7% compromising charge generation and recombination of organic photovoltaics with mixed diluent strategy for certified 19.4% efficiency, Adv. Mater. 35 (2023) 2300400 https://onlinelibrary.wiley.com/doi/abs/10.1002/adma.202300400.
[10] G. Zhang, F.R. Lin, F. Qi, T. Heumüller, A. Distler, H.-J. Egelhaaf, N. Li, P.C. Y. Chow, C.J. Brabec, A.K.Y. Jen, H.-L. Yip, Renewed prospects for organic photovoltaics, Chem. Rev 122 (2022) 14180–14274, https://doi.org/10.1021/acs.chemrev.1c00955.
[11] J. Wang, Z. Zheng, Y. Zu, Y. Wang, X. Liu, S. Zhang, M. Zhang, J. Hou, A Tandem Organic Photovoltaic Cell with 19.6% Efficiency Enabled by Light Distribution Control, Adv. Mater. 33 (2021) 2102787 https://onlinelibrary.wiley.com/doi/abs/10.1002/adma.202102787.
[12] S. Liu, J. Yuan, W. Deng, M. Luo, Y. Xie, Q. Liang, Y. Zou, Z. He, H. Wu, Y. Cao, High-efficiency organic solar cells with low non-radiative recombination loss and low energetic disorder, Nat. Photonics 14 (2020) 300–305, https://doi.org/10.1038/s41566-019-0573-5.
[13] J. Yan, Q. Liang, K. Liu, J. Miao, H. Chen, S. Liu, Z. He, H. Wu, J. Wang, Y. Cao, Optimized phase separation and reduced geminate recombination in high fill factor small-molecule organic solar cells, ACS Energy Lett. 2 (2017) 14–21, https://doi.org/10.1021/acsenergylett.6b00556.
[14] P. Bi, J. Wang, Y. Cui, J. Zhang, T. Zhang, Z. Chen, J. Qiao, J. Dai, S. Zhang, X. Hao, Z. Wei, J. Hou, Enhancing photon utilization efficiency for high-performance organic photovoltaic cells via regulating phase-transition kinetics, Adv. Mater. 35 (2023) 2210865 https://onlinelibrary.wiley.com/doi/abs/10.1002/adma.202210865.
[15] J. Wang, Y. Wang, P. Bi, Z. Chen, J. Qiao, J. Li, W. Wang, Z. Zheng, S. Zhang, X. Hao, J. Hou, Binary organic solar cells with 19.2% efficiency enabled by solid additive, Adv. Mater. 35 (2023) 2301583, https://doi.org/10.1002/adma.202301583.
[16] H.-C. Liao, C.-C. Ho, C.-Y. Chang, M.-H. Jao, S.B. Darling, W.-F. Su, Additives for morphology control in high-efficiency organic solar cells, Mater. Today 16 (2013) 326–336, https://doi.org/10.1016/j.mattod.2013.08.013.
[17] R.N. Yu, H.F. Yao, L. Hong, Y.P. Qin, J. Zhu, Y. Cui, S.S. Li, J.H. Hou, Design and application of volatilizable solid additives in non-fullerene organic solar cells, Nat. Commun. 9 (2018), https://doi.org/10.1038/s41467-018-07017-z.
[18] X. Guo, Q. Fan, J. Wu, G. Li, Z. Peng, W. Su, J. Lin, L. Hou, Y. Qin, H. Ade, L. Ye, M. Zhang, Y. Li, Optimized morphologies via ternary copolymerization 17.6%, Angew. Chem., . Ed. 60 (2021) 2322–2329, https://onlinelibrary.wiley.com/doi/abs/10.1002/anie.202010596.
[19] J. Fu, P.W.K. Fong, H. Liu, C.-S. Huang, X. Lu, S. Lu, M. Abdelsamie, T. Kodalle, C. M. Sutter-Fella, Y. Yang, G. Li, 19.31% PM6:Y6 binary organic solar cell and low non-radiative recombination enabled by non-monotonic intermediate state

transition, Nat. Commun. 14 (2023) 1760, https://doi.org/10.1038/s41467-023-37526-5.
[20] R. Yu, H. Yao, L. Hong, Y. Qin, J. Zhu, Y. Cui, S. Li, J. Hou, Design and application of volatilizable solid additives in non-fullerene organic solar cells, Nat. Commun. 9 (2018), https://doi.org/10.1038/s41467-018-07017-z.
[21] J. Song, Y. Li, Y. Cai, R. Zhang, S. Wang, J. Xin, L. Han, D. Wei, W. Ma, F. Gao, Y. Sun, Solid additive engineering enables high-efficiency and eco-friendly all-polymer solar cells, Matter 5 (2022) 4047–4059, https://doi.org/10.1016/j.matt.2022.08.011.
[22] L. Zhang, Z. Zhang, D. Deng, H. Zhou, J. Zhang, Z. Wei, "N-π-N" type oligomeric acceptor achieves an OPV efficiency of 18.19% with low energy loss and excellent stability, Adv. Sci. 9 (2022) 2202513 https://onlinelibrary.wiley.com/doi/abs/10.1002/advs.202202513.
[23] C. Sun, J.-W. Lee, C. Lee, D. Lee, S. Cho, S.-K. Kwon, B.J. Kim, Y.-H. Kim, Dimerized small-molecule acceptors enable efficient and stable organic solar cells, Joule 7 (2023) 416–430, https://doi.org/10.1016/j.joule.2023.01.009.
[24] X. Gu, Y. Wei, N. Yu, J. Qiao, Z. Han, Q. Lin, X. Han, J. Gao, C. Li, J. Zhang, X. Hao, Z. Wei, Z. Tang, Y. Cai, X. Zhang, H. Huang, High-efficiency and low-energy-loss organic solar cells enabled by tuning conformations of dimeric electron acceptors, CCS Chem. 5 (2023) 2576–2588, https://www.chinesechemsoc.org/doi/abs/10.31635/ccschem.023.202202575.
[25] Y. Bai, Z. Zhang, Q. Zhou, H. Geng, Q. Chen, S. Kim, R. Zhang, C. Zhang, B. Chang, S. Li, H. Fu, L. Xue, H. Wang, W. Li, W. Chen, M. Gao, L. Ye, Y. Zhou, Y. Ouyang, C. Zhang, F. Gao, C. Yang, Y. Li, Z.-G. Zhang, Geometry design of tethered small-molecule acceptor enables highly stable and efficient polymer solar cells, Nat. Commun. 14 (2023) 2926, https://doi.org/10.1038/s41467-023-38673-5.
[26] X. Yang, B. Li, X. Zhang, S. Li, Q. Zhang, L. Yuan, D.H. Ko, W. Ma, J. Yuan, Intrinsic role of volatile solid additive in high-efficiency PM6:Y6 series nonfullerene solar cells, Adv. Mater. 35 (2023).
[27] Z. Li, K. Jiang, G. Yang, J.Y.L. Lai, T. Ma, J. Zhao, W. Ma, H. Yan, Donor polymer design enables efficient non-fullerene organic solar cells, Nat. Commun. 7 (2016) 13094, https://doi.org/10.1038/ncomms13094.
[28] R. Yu, H. Yao, Z. Chen, J. Xin, L. Hong, Y. Xu, Y. Zu, W. Ma, J. Hou, Enhanced π–π interactions of nonfullerene acceptors by volatilizable solid additives in efficient polymer solar cells, Adv. Mater. 31 (2019) 1900477 https://onlinelibrary.wiley.com/doi/abs/10.1002/adma.201900477.
[29] J. Qu, H. Chen, J. Zhou, H. Lai, T. Liu, P. Chao, D. Li, Z. Xie, F. He, Y. Ma, Chlorine atom-induced molecular interlocked network in a non-fullerene acceptor, ACS Appl. Mater. Interfaces 10 (2018) 39992–40000, https://doi.org/10.1021/acsami.8b15923.
[30] W. Feng, T. Chen, Y. Li, T. Duan, X. Jiang, C. Zhong, Y. Zhang, J. Yu, G. Lu, X. Wan, B. Kan, Y. Chen, Binary all-polymer solar cells with a perhalogenated-thiophene-based solid additive surpass 18% efficiency, Angew. Chem., Int. Ed. (2024) e202316698 https://onlinelibrary.wiley.com/doi/abs/10.1002/anie.202316698.
[31] Z. Gan, L. Wang, J. Cai, C. Guo, C. Chen, D. Li, Y. Fu, B. Zhou, Y. Sun, C. Liu, J. Zhou, D. Liu, W. Li, T. Wang, Electrostatic force promoted intermolecular stacking of polymer donors toward 19.4% efficiency binary organic solar cells, Nat. Commun. 14 (2023) 6297, https://doi.org/10.1038/s41467-023-42071-2.
[32] J.-W. Lee, C. Sun, C. Lee, Z. Tan, T.N.-L. Phan, H. Jeon, D. Jeong, S.-K. Kwon, Y.-H. Kim, B.J. Kim, Linker engineering of dimerized small molecule acceptors for highly efficient and stable organic solar cells, ACS Energy Lett. 8 (2023) 1344–1353, https://doi.org/10.1021/acsenergylett.2c02679.
[33] J. Song, C. Li, J. Qiao, C. Liu, Y. Cai, Y. Li, J. Gao, M.H. Jee, X. Hao, H.Y. Woo, Z. Tang, H. Yan, Y. Sun, Over 18% efficiency ternary all-polymer solar cells with high photocurrent and fill factor, Matter 6 (2023) 1542–1554, https://doi.org/10.1016/j.matt.2023.03.001.
[34] C. Li, J. Zhou, J. Song, J. Xu, H. Zhang, X. Zhang, J. Guo, L. Zhu, D. Wei, G. Han, J. Min, Y. Zhang, Z. Xie, Y. Yi, H. Yan, F. Gao, F. Liu, Y. Sun, Non-fullerene acceptors with branched side chains and improved molecular packing to exceed 18% efficiency in organic solar cells, Nat. Energy 6 (2021) 605–613, https://doi.org/10.1038/s41560-021-00820-x.
[35] J. Liu, W. Zhou, J. Deng, X. Geng, S.Y. Jeong, Y. Cui, H.Y. Woo, F. Wu, F. Liu, L. Chen, Dimerized small molecular acceptors: Regulation of dimer conformation realizes binary organic solar cells with highly comprehensive performance, Nano Energy 121 (2024), https://doi.org/10.1016/j.nanoen.2023.109218.
[36] Y. Li, J. Song, Y. Dong, H. Jin, J. Xin, S. Wang, Y. Cai, L. Jiang, W. Ma, Z. Tang, Y. Sun, Polymerized small molecular acceptor with branched side chains for all polymer solar cells with efficiency over 16.7, Adv. Mater. 34 (2022) 2110155 https://onlinelibrary.wiley.com/doi/abs/10.1002/adma.202110155.
[37] L. Zhong, S. Jeong, S. Lee, T.L.H. Mai, J. Park, J. Park, W. Kim, C. Yang, Octafluoronaphthalene as a thermal-annealing-free volatile solid additive enables high-performance organic solar cells, Chem. Commun. 59 (2023) 12108–12111, https://doi.org/10.1039/D3CC03827K.
[38] M. Xiao, Y. Meng, L. Tang, P. Li, L. Tang, W. Zhang, B. Hu, F. Yi, T. Jia, J. Cao, C. Xu, G. Lu, X. Hao, W. Ma, Q. Fan, Solid Additive-Assisted Selective Optimization Strategy for Sequential Deposited Active Layers to Construct 19.16% Efficiency Binary Organic Solar Cells, Adv. Funct. Mater. n/a 2311216. https://onlinelibrary.wiley.com/doi/abs/10.1002/adfm.202311216.
[39] X. Zhang, C. Li, J. Xu, R. Wang, J. Song, H. Zhang, Y. Li, Y.-N. Jing, S. Li, G. Wu, J. Zhou, X. Li, Y. Zhang, X. Li, J. Zhang, C. Zhang, H. Zhou, Y. Sun, Y. Zhang, High fill factor organic solar cells with increased dielectric constant and molecular packing density, Joule 6 (2022) 444–457, https://doi.org/10.1016/j.joule.2022.01.006.
[40] X. Meng, M. Li, K. Jin, L. Zhang, J. Sun, W. Zhang, C. Yi, J. Yang, F. Hao, G.-W. Wang, Z. Xiao, L. Ding, A 4-arm small molecule acceptor with high photovoltaic performance, Angew. Chem., . Ed. 61 (2022) e202207762 https://onlinelibrary.wiley.com/doi/abs/10.1002/anie.202207762.
[41] J. Wan, T. Wang, R. Sun, X. Wu, S. Wang, M. Zhang, J. Min, Enabling highly efficient and thermal-stable polymer solar cells through semi-alloy acceptors composed of a hinge-like dimer: a versatile doping protocol, Adv. Mater. 35 (2023) 2302592 https://onlinelibrary.wiley.com/doi/abs/10.1002/adma.202302592.
[42] F. Qi, Y. Li, R. Zhang, F.R. Lin, K. Liu, Q. Fan, A.K.-Y. Jen, Dimer acceptor adopting a flexible linker for efficient and durable organic solar cells, Angew. Chem. 62 (2023) e202303066 https://onlinelibrary.wiley.com/doi/abs/10.1002/anie.202303066.
[43] H. Chen, Y. Zou, H. Liang, T. He, X. Xu, Y. Zhang, Z. Ma, J. Wang, M. Zhang, Q. Li, C. Li, G. Long, X. Wan, Z. Yao, Y. Chen, Lowing the energy loss of organic solar cells by molecular packing engineering via multiple molecular conjugation extension, Sci. China Chem. 65 (2022) 1362–1373, https://doi.org/10.1007/s11426-022-1264-y.
[44] V.D. Mihailetchi, L.J.A. Koster, J.C. Hummelen, P.W.M. Blom, Photocurrent generation in polymer-fullerene bulk heterojunctions, Phys. Rev. Lett. 93 (2004) https://10.1103/PhysRevLett.93.216601.
[45] J. Rivnay, S.C.B. Mannsfeld, C.E. Miller, A. Salleo, M.F. Toney, Quantitative determination of organic semiconductor microstructure from the molecular to device scale, Chem. Rev. 112 (2012) 5488–5519, https://10.1021/cr3001109.
[46] J. Song, M. Zhang, M. Yuan, Y. Qian, Y. Sun, F. Liu, Morphology characterization of bulk heterojunction solar cells, Small Methods 2 (2018) 1700229 https://onlinelibrary.wiley.com/doi/abs/10.1002/smtd.201700229.
[47] L. Wen, H. Mao, L. Zhang, J. Zhang, Z. Qin, L. Tan, Y. Chen, Achieving desired pseudo-planar heterojunction organic solar cells via binary-dilution strategy, Adv. Mater. 36 (2024) 2308159 https://onlinelibrary.wiley.com/doi/abs/10.1002/adma.202308159.
[48] J. Yu, Z. Shen, W. Lu, Y. Zhu, Y.-X. Liu, D. Neher, N. Koch, G. Lu, Composition waves in solution-processed organic films and its propagations from kinetically frozen surface mesophases, Adv. Funct. Mater. 33 (2023) 2302089 https://onlinelibrary.wiley.com/doi/abs/10.1002/adfm.202302089.